Kyle, S., Jessop, Z. M., Al-Sabah, A., Hawkins, K., Lewis, A., Maffeis, T., Charbonneau, C., Gazze, A., Francis, L. W., Iakovlev, M., Nelson, K., Eichhorn, S. J., & Whitaker, I. S. (2018). Characterization of pulp derived nanocellulose hydrogels using AVAP® technology. *Carbohydrate Polymers*, *198*, 270-280. https://doi.org/10.1016/j.carbpol.2018.06.091

Characterization of Pulp Derived Nanocellulose Hydrogels using AVAP® Technology

Stuart Kyle[1,2,*,+], Zita M. Jessop[1,2,+], Ayesha Al-Sabah[1], Karl Hawkins[3], Aled Lewis[4], Thierry Maffeis[4], Cecile Charbonneau[5], Andrea Gazze[3], Lewis W. Francis[3], Mikhail Iakovlev[6], Kim Nelson[6], Stephen J. Eichhorn[7], Iain S. Whitaker[1,2,*]

[1]Reconstructive Surgery & Regenerative Medicine Group (ReconRegen), Institute of Life Sciences, Swansea University Medical School, Swansea, SA2 8PP, UK
[2]The Welsh Centre for Burns and Plastic Surgery, Morriston Hospital, Swansea, SA6 6NL, UK
[3]Centre for NanoHealth, Swansea University, Singleton Campus, Swansea, SA2 8PP, UK
[4]Systems and Process Engineering Centre, College of Engineering, Swansea University, Fabian Way, Swansea, SA1 8EN, UK
[5]SPECIFIC, College of Engineering, Swansea University, Baglan Bay Innovation and Knowledge Centre, Port Talbot, SA12 7AQ, UK
[6]American Process Inc, Atlanta, GA 30308, USA
[7]Bristol Composites Institute (ACCIS), University of Bristol, Queen's Building, University Walk, Bristol, BS8 1TR, UK
* Corresponding authors.
+ these authors contributed equally to this work.

Email addresses: stuart.kyle@doctors.org.uk (S. Kyle), zitajessop@gmail.com (Z. M. Jessop), aishaalsabah@yahoo.com (A. Al-Sabah), K.M.Hawkins@Swansea.ac.uk (K. Hawkins), 557952@swansea.ac.uk (A. Lewis), T.G.G.Maffeis@Swansea.ac.uk (T. Maffeis), C.M.E.Charbonneau@Swansea.ac.uk (C. Charbonneau), S.A.Gazze@Swansea.ac.uk (A. Gazze), l.francis@swansea.ac.uk (L. Francis), miakovlev@americanprocess.com (M. Iakovlev), knelson@americanprocess.com (K. Nelson), s.j.eichhorn@bristol.ac.uk (S. J. Eichhorn), iainwhitaker@fastmail.fm (I. S. Whitaker)

ABSTRACT

Bioinspiration from hierarchical structures found in natural environments has heralded a new age of advanced functional materials. Nanocellulose has received significant attention due to the demand for high-performance materials with tailored mechanical, physical and biological properties. In this study, nanocellulose fibrils, nanocrystals and a novel mixture of fibrils and nanocrystals (blend) were prepared from softwood biomass using the AVAP® biorefinery technology. These materials were characterized using transmission and scanning electron microscopy, and atomic force microscopy. This analysis revealed a nano- and microarchitecture with extensive porosity. Notable differences included the nanocrystals exhibiting a compact packing of nanorods with reduced porosity. The NC blend exhibited porous fibrillar networks with interconnecting compact nanorods. Fourier transform infrared spectroscopy and X-ray diffraction confirmed a pure cellulose I structure. Thermal studies highlighted the excellent stability of all three NC materials with the nanocrystals having the highest decomposition temperature. Surface charge analysis revealed stable colloid suspensions. Rheological studies highlighted a dominance of elasticity in all variants, with the NC blend being more rigid than the NC fibrils and nanocrystals, indicating a double network hydrogel structure. Given these properties, it is thought that these materials show great potential in (bio)nanomaterial applications where careful control of microarchitecture, surface topography and porosity are required.

Keywords

Nanocellulose; nanofibrils; nanocrystals; blends; characterization

1. Introduction

Bioinspiration from complex, hierarchical structures found in natural, biological molecules is a useful tool to aid scientists develop contemporary advanced functional materials for a plethora of applications. Of these, cellulose has received much attention due to increased demand for high-performance materials with tailored mechanical, physical and biological properties (Abitbol et al., 2016). Cellulose, a polysaccharide composed of D-glucopyranose linked by β–1,4 glycosidic bonds (Endes et al., 2016), is the most abundant, renewable and biodegradable polymer in the world, found in plant cell walls, algae, marine organisms and bacteria. By natural, photosynthetic processes, plants synthesise cellulose, accounting for approximately 40% of lignocellulosic biomass. Cellulose has three hydroxyl groups (-OH): a primary hydroxyl at the C-6 position, and two secondary hydroxyls at the C-2 and C-3 positions, which play an important role in the compactness of the crystalline structure and determine its physical properties. Extensive inter- and intramolecular hydrogen bonding between –OH groups imparts structural integrity and mechanical strength to the material.

Nanocellulose (NC) is an emerging class of advanced nanomaterials possessing unique physical, structural, chemical and biological properties. NC can be divided into three types of materials: (i) biomass-based cellulose nanocrystals (CNCs) or nanowhiskers, (ii) biomass-based cellulose nanofibrils, and (iii) bacterial cellulose nanofibrils. Hybrid composite blends can also be created where CNCs and fibrils are mixed to enhance physicochemical and biological properties, making them more suited to certain applications. Unique properties of NC include extraordinarily high stiffness (100-200 GPa) and strength, low density, flexibility, reactive surfaces, functionalisability, high surface area and aspect ratio, excellent biocompatibility and non-toxicity. As a result, NC research in the last decade has grown exponentially.

Production of NC range from ‘top-down’ approaches involving chemical, mechanical and/or enzymatic (Yarbrough et al., 2017) methods which can isolate the materials from wood and agricultural residues, to ‘bottom-up’ methods using bacteria to produce cellulose from glucose. The resulting nanoparticles offer unique properties with varied surface chemistry, crystallinities and mechanical properties (Abitbol et al., 2016). Mechanical processing, typically through refining or homogenization, is

relatively simple but has high energy consumption. Chemical pre-treatments, such as applying 2,2,6,6-tetramethylpiperidine-1-oxyl (TEMPO) functionality before mechanical treatment can minimise energy consumption. However, methods like TEMPO are associated with increased consumable costs. Bacterial cellulose has its uses (Markstedt et al., 2015) and can be produced with high purity, free from lignin and hemicelluloses. Bacterial cellulose has shown promise for tissue engineering applications due to its biocompatibility, nanostructure, water-holding capacity, high strength and morphological similarities to collagen, thereby providing good cell support (Ahrem et al., 2014; Dugan, Gough, & Eichhorn, 2013; Markstedt et al., 2015; Paakko et al., 2007). Several studies have also demonstrated that the rheological properties of bacterial cellulose make it a suitable bioink for 3D bioprinting. However, the major drawbacks of high substrate costs, low yield of NC products and concerns regarding residual bacterial toxins/epitopes makes this method less desirable and warrants investigation of alternative sources if NC is to become a commercially viable biomaterial (Paakko et al., 2007).

Acid hydrolysis is the most widespread chemical method to extract nanocellulose from lignocellulosic biomass (Lin, Bruzzese, & Dufresne, 2012), creating CNCs/nanowhiskers from cellulose fibers (hydrolysis of the less ordered domains of cellulose with persisting intact crystalline domains) (Abdul Khalil, Bhat, & Ireana Yusra, 2012). The hydrolysis kinetics between crystalline and amorphous regions of cellulose are different, leading to hydrolysis of the amorphous regions and production of CNCs (Habibi, Lucia, & Rojas, 2010).

NC produced using American Value Added Pulping (AVAP®) technology chemically pre-treats the wood-pulp derived biomass to remove hemicelluloses, lignin and the amorphous regions of cellulose (Nelson & Retsina, 2014). Lignin is separated from cellulose and hemicelluloses using the delignifying agent, sulfur dioxide. Mechanisms of this process have previously been reported (Iakovlev, You, van Heiningen, & Sixta, 2014). Resins and extractives are dissolved using ethanol. In addition, the degradation of crystalline cellulose is also reduced (Nelson & Retsina, 2014). During the delignification process, strong lignosulfonic acids help hydrolyse the amorphous regions of cellulose (Nelson & Retsina, 2014). Fractionation to NC fibrils dissolves approximately 90% of lignin and 90% hemicelluloses, whilst fractionation to CNCs additionally hydrolyses amorphous cellulose (approximately half of cellulose). However, lignin-carbohydrate complex is hydrolysed in both cases and the

fractionation liquor contains dissolved lignin, lignosulfonic acids and hemicellulose sugars. The resulting NC yield (with respect to softwood biomass, NC fibrils: 40 – 60%; CNCs: 20 – 30%; NC blend: intermediate yield values) and morphology depends on optimized experimental parameters such as time and temperature. The AVAP® process is based on the “tunability” of the pre-treatment step. For each feedstock, the pre-treatment conditions (time and temperature) are selected to give the desired levels of fibrillation and removal of amorphous cellulose, as indicated by the degree of polymerization (DP). American Process Inc. (API), GA, USA have shown, using eucalyptus, softwood and cane straw, that two unique DP targets exist for the production of NC fibrils and CNCs after mechanical treatment. Between the two targets, a blend of NC fibrils and CNCs is produced (Nelson & Retsina, 2014; Nelson et al., 2016). The morphological structure of NC is highly dependent on the efficient removal of non-cellulosic regions and hydrolysis of amorphous domains (Lu et al., 2013; Mondal, 2017). Hence AVAP technology is a sustainable platform that uses low cost raw biomass and pre-treatment chemicals, a small number of process steps, low operating and capital costs, low energy consumption and creates revenue from the ethanol co-product (Nelson & Retsina, 2014; Nelson et al., 2016).

Although the cellulose molecular backbone is common to all; surface morphology, size, chemical and physical properties can vary greatly depending upon the material source and extraction methods used (Mao et al., 2017). The objective of this study was to examine the physicochemical properties of NC fibrils, CNCs and a novel blend of these materials produced via the AVAP® technology. The product containing fibrils and CNCs is produced *in situ* during production and is not a *de facto* blending of separate fibrils and CNC products. However, it is herein referred to as a blend for simplicity. The physical properties of these materials were characterized in terms of surface morphology (TEM, AFM and cryoSEM), chemical functional groups (FTIR), crystalline structure (XRD), thermal stability (TGA) and rheology. Determining these properties is a key aspect for structure-function relationships which could widen NC applications. For example, assessing physicochemical properties enables better prediction of cellular interactions when considering the use of NC as a biomaterial for tissue engineering. It is also important when planning functionalization with biologically active groups to improve biocompatibility and tissue generation. Linking NC structure and surface chemistry with the rheological properties of the material may also allow

fine tuning of the biomaterial for 3D bioprinting applications (Kyle, Jessop, Al-Sabah, & Whitaker, 2017).

2. Materials and Methods

2.1. Production of NC fibrils, crystals and blend

NC fibrils and CNCs were produced from wood chips using the patented AVAP® technology which fractionates biomass into cellulose, hemicelluloses and lignin using ethanol and sulfur dioxide. NC products were processed by American Process Inc, Atlanta, GA (Nelson & Retsina, 2014; Nelson et al., 2016; Nelson, Retsina, Pylkkanen, & O'Connor, 2015). The final nanocellulose product morphology (NC fibrils (3 wt.% solids), CNCs (6 wt.% solids), or a novel blend of NC fibrils and CNCs (3 wt.% solids)) was controlled by the time and temperature (i.e. severity) of the pre-treatment step.

2.2. Transmission electron microscopy (TEM)

Each sample (2 mg) was dispersed in 5 mL of deionized water and sonicated for 30 minutes. After sonication 50 µL of the sample was immediately taken and further dispersed into 1 mL of deionized water to prevent coalescence. This solution (10 µL) was added to 300 mesh copper grids coated with lacey carbon film. The grid was allowed to air dry prior to staining with a 1.5% uranyl acetate solution. For staining, a drop of the uranyl acetate solution was placed on a parafilm strip and the grid inverted onto the droplet for a few seconds. The samples were then allowed to air dry. Analysis was performed on a Jeol 2100 TEM operating at 200 kV.

2.3. Atomic force microscopy (AFM)

A Bruker BioScope Catalyst (Bruker Instruments, Santa Barbara, California, USA) was used to visualize fibrils deposited on freshly-cleaved mica flakes. 150 µL of aqueous fibril solution was deposited on mica, left to air-dry at room temperature and subsequently scanned with AFM in air. MPP-21200-10 cantilevers (Bruker Instruments, Santa Barbara, California, USA) were used, with a nominal spring

constant of 3 N/m and a nominal resonant frequency of 75 kHz. All imaging was conducted using Peak Force Tapping Mode at a scan speed of 1 Hz. Images were processed with first-order flattening and the dimensions of objects were calculated using Bruker Nanoscope Analysis software and ImageJ software.

AFM topographical data was also used to quantify roughness on several sub-regions of 250 x 10^3 nm^2 on three different 25 μm^2 areas for all NC materials. The roughness sub-routine in the Nanoscope Analysis software v1.50 was adopted, which calculates roughness using the following equation:

$$R_{RMS} = \sqrt{\frac{\sum Z_i^2}{N}} \quad (1)$$

where R_{RMS} is roughness (root mean square), Z_i is the vertical distance of data point *i* from the mean image data plane and *N* is the number of height points in the analysed area. A minimum of 40 data points were considered for each NC material. Data distribution was evaluated using the Anderson-Darling (AD) test for normality and, since the roughness for all NC materials displayed a normal behaviour ($p > 0.05$), a t-test was applied to evaluate any statistical differences.

2.4. Cryo-scanning electron microscopy (cryo-SEM)

Electron microscopy was carried out using a Hitachi S4800 field emission scanning electron microscope equipped with a Quorum PPT2000 cryogenic stage. The nano-cellulose samples were drop cast onto the SEM sample holder which was then plunged into nitrogen slush and loaded into a cryogenic preparation chamber held at -160 °C via a vacuum capsule. The samples were slowly cooled to -90 °C for 10 min in order to sublimate any surface ice, and then coated in platinum (ca. 5 nm) prior to transfer to the SEM chamber. Imaging was performed at -120 °C.

2.5. Fourier-transform infra-red spectroscopy (FTIR)

FTIR experiments were conducted using a PerkinElmer Spectrum Two™ FTIR spectrometer with a lithium tantalite infra-red detector and Universal Diamond attenuated total reflectance attachment (PerkinElmer, London, UK). The spectra were

recorded in the range from 3600 to 500 cm^{-1} at 4 cm^{-1} resolution and 64 scans per spectrum in the transmission mode.

2.6. X-ray diffraction (XRD)

Samples were prepared on a microscope glass slides and allowed to dry in a silica desiccator for 72 hours. XRD data of dried nanocellulose was acquired using a D8 Discover X-ray diffractometer (Bruker Ltd.) with Cu Kα (0.154 nm) radiation generated at 40 kV and 40 mA. The scan parameters were set at 2 s per step with 0.05 ° step resolution in the range of 2θ. Subtraction of background intensity from the measure intensity of nanocellulose samples was performed.

2.7. Thermogravimetric analysis (TGA)

The thermal stability of samples was analyzed using a thermal gravimetric analyzer (PerkinElmer STA6000 Simultaneous Thermal Analyzer, London, UK). All samples were heated from 50 to 600 °C at a heating rate of 10 °C.min^{-1} under nitrogen atmosphere with a flow rate of 40 ml.min^{-1}.

2.8. Surface charge analysis

Zeta potential measurements (estimated as surface charge) were carried out using a Zetasizer NanoZS (Malvern Instruments, UK). The supernatants obtained after centrifugation of 2 ml of the NC suspensions (5 % (w/v)) at 5000 rpm for 30 min were analyzed. Measurements were performed in 10 steps using a Universal Dip Cell (Malvern Instruments, UK) in a cuvette, and results were an average of five replicates.

2.9. Rheology

The rheological properties of each sample (fibrils, crystals and blend) were measured using an AR-G2 (TA instruments, UK) Controlled Stress Rheometer fitted with a 40 mm diameter parallel plate geometry. Prior to each experiment, the rheometers' zero gap was set and the geometry was calibrated using rotational

mapping. Approximately 1 ml of sample was carefully loaded using a spatula onto the center of the lower plate of the rheometer and the upper plate was gradually lowered onto the sample until the gap was totally filled (gaps ranged from 700 – 1000 µm). Any excess sample around the edge of the geometry was trimmed using a spatula. The normal force measured at the lower plate was set at a maximum of 0.1 N to ensure that any mechanical damage to the sample during gap setting procedure was minimized. The rheometers' lower plate was controlled at a temperature of 22 °C and a vapour hood was used in order to reduce sample evaporation.

Following a sample equilibration period of 5 min, a frequency sweep (0.1 to 10 Hz) was performed at a constant stress of 0.01 Pa. Each measurement was within the linear viscoelastic range of the sample as confirmed by the absence of a third harmonic in the strain response waveform. Values of storage modulus (G') and loss modulus (G'') were recorded over the entire frequency range employed. At the end of the frequency sweep, a shear flow ramp was carried out on the same sample at logarithmically increasing shear rates in the range of 0.1 – 100 s^{-1} over a period of 2 min. These sets of experiments were repeated 5 times for each sample.

3. Results and Discussion

3.1. Morphological properties.

3.1.1. Nanoparticle size.

The nanoparticle sizes were found from electron microscopy images using TEM (**Fig. 1**), AFM (**Fig. 2**) and Cryo-SEM (**Fig. 3**). These techniques were used to observe the morphology of NC fibrils, CNCs and a blend.

TEM and image analysis software were used to measure the widths and lengths of the materials (**Table 1**), with Fig. 1 and 2 highlighting the architecture of the NC fibrils (Fig. 1A-D; Fig. 2A-C). Very long and thin nanofibers with varying degrees of entanglements can be seen. It was evident from TEM and AFM imaging that agglomeration occurred with parallel arrangements of nanostructures as reported in other studies (Kvien, Tanem, & Oksman, 2005). The widths of nanofibers were found to be in the range of 6 – 90 nm, with a mean width of 29 ± 18 nm (Table 1). Widths of

single elemental fibrils have been reported to be as small as 3 nm when isolated from plant cell walls (Somerville et al., 2004). Lengths of nanofibers ranged from 212 – 4513 nm, with mean lengths of 1627 ± 1252 nm and a high aspect ratio of 55, which is greater than or equal to values previously reported (Cheng, Wang, Rials, & Lee, 2007; Zhou, Fu, Zheng, & Zhan, 2012). High aspect ratios enhance the reinforcing effect of materials, which can result in improved mechanical properties. For example, studies have also shown that the high aspect ratio of NC may facilitate an increase in fracture toughness for cement composites (Sun, Wu, Lee, Qing, & Wu, 2016). Measurement of the lengths of NC fibrils using microscopic techniques was difficult, as many of the fibrils formed larger cellulosic entanglements. Aspect ratio plays an important role in the formation of percolated networks that improve the mechanical performances of polymer nanocomposites (Peng, Dhar, Liu, & Tam, 2011); aspect ratios >500 of NC fibers have been reported through careful control of mechanical and chemical parameters in the extraction process (Amiralian et al., 2015). Nanomaterials with higher aspect ratios generally show better reinforcing ability, however, nanofibrils are known to form bundles, and their ends can be difficult to observe and measure using TEM alone due to their entangled, web-like structures (W. Chen et al., 2015).

Observation of CNCs showed rod-like networks which were clearly visible (Fig. 1 E-H; Fig. 2D-F). These CNCs exhibited widths which ranged from 2 – 9 nm, with a mean width of 4.5 ± 1.5 nm (Table 1). Lengths ranged from 44 – 571 nm, with a mean length of 222 ± 139 nm. CNCs also exhibited high aspect ratios of 49, in line with previous studies (Roohani et al., 2008; Rosa et al., 2010). Aspect ratios of CNCs reported in this study were higher than previously reported, where different sources of materials and extraction methods have been employed (Cho & Park, 2011; Nascimento et al., 2014).

Due to the rigid, relatively straight and highly crystalline nature of CNCs with high aspect ratios, they have shown great potential in a range of applications from barrier films and coatings in packaged foods to tissue engineering. Extensive hydrogen bonding has also been shown to promote very efficient stress transfer which makes CNCs ideal candidates as reinforcing fillers in polymers (Capadona, Shanmuganathan, Tyler, Rowan, & Weder, 2008; Endes et al., 2016). Moreover, the hydrogen bonding capability can be manipulated on demand via switch off mechanisms through competing hydrogen bonding forming agents which has led to

the fabrication of stimuli-responsive materials (Capadona et al., 2008; Capadona et al., 2007; Endes et al., 2016; Shanmuganathan, Capadona, Rowan, & Weder, 2010).

Images of the blend show a combination of the two types of structures (Fig. 1I-L; Fig. 2G-I). Resulting nanostructures therefore showed a mean width of 17 ± 12 nm, and long nanofibers with a mean length of 925 ± 787 nm and an aspect ratio of ~55.

TEM and AFM images of the NC blend clearly showed fibrillar entanglements of NC nanofibrils interspersed with CNCs. This is especially evident in Fig. 2I where twisted nanofibrils are seen surrounded by smaller clusters of well-defined nanocrystals. It was evident that a blend of fibrils and crystals led to unique morphologies, which could potentially broaden their fields of application. This difference in morphology is quantitatively evaluated through roughness measurements using the 3D topographical data obtained with AFM (Figure 2J). NC crystals presented a nano-roughness of 10.8 ± 2.5 nm, significantly different from both NC fibrils and the NC blend (13.1 ± 4.8 nm and 13.4 ± 4.1 nm, respectively), which had the same roughness (t-test $p > 0.05$). It has been previously demonstrated, through various characterization techniques, that incorporation of CNCs into biopolymers can result in bionanocomposite materials with enhanced physicochemical properties (Kamal & Khoshkava, 2015), however a blend of nanocrystals and fibrils has not been reported to our knowledge.

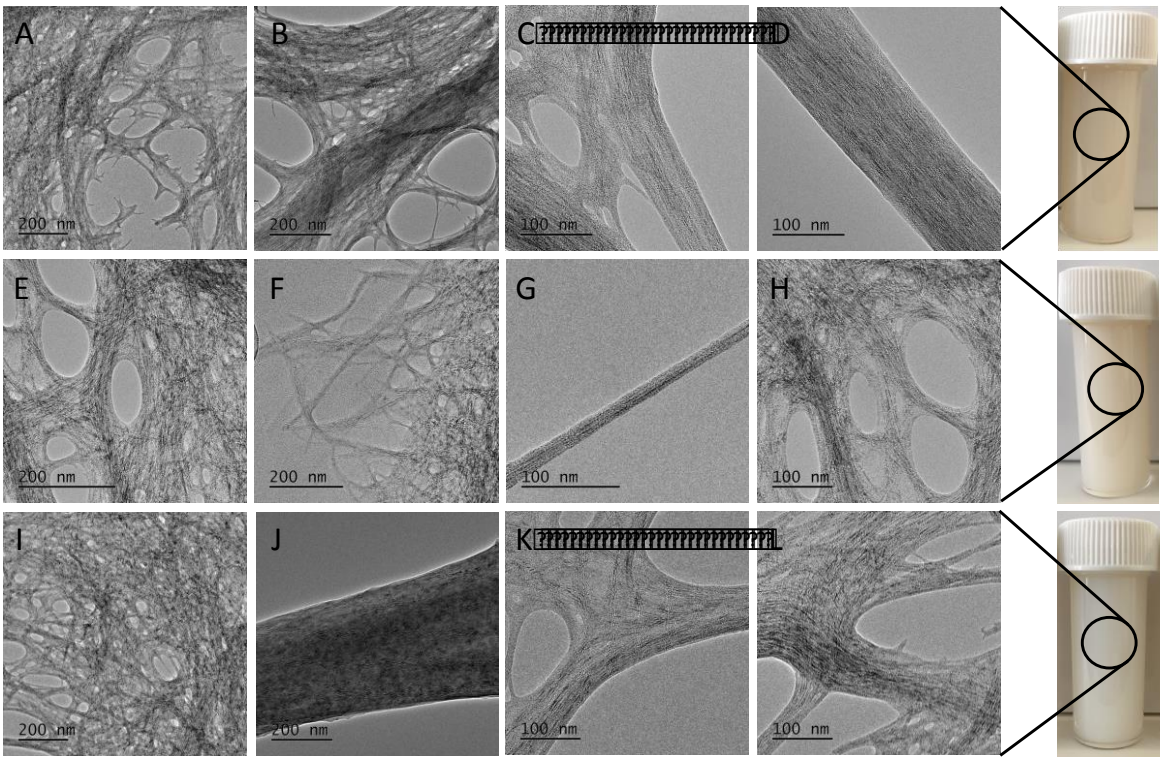

Fig. 1. TEM analysis of **(A-D)** NC fibrils, **(E-H)** CNCs and **(I-L)** NC blend.

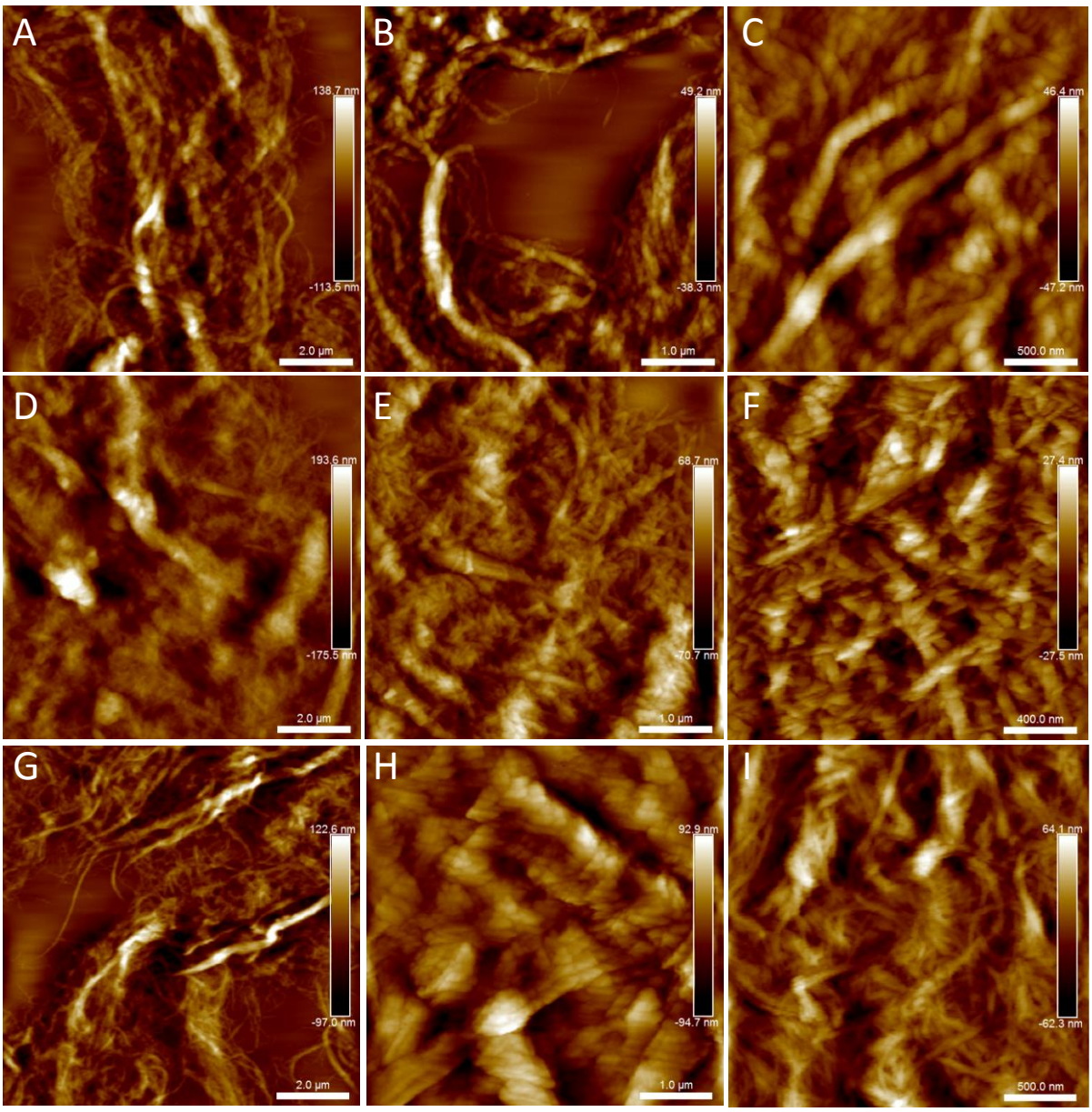
A
138.7 nm
-113.5 nm
2.0 µm
B
49.2 nm
-38.3 nm
1.0 µm
C
46.4 nm
-47.2 nm
500.0 nm
D
193.6 nm
-175.5 nm
2.0 µm
E
68.7 nm
-70.7 nm
1.0 µm
F
27.4 nm
-27.5 nm
400.0 nm
G
122.6 nm
-97.0 nm
2.0 µm
H
92.9 nm
-94.7 nm
1.0 µm
I
64.1 nm
-62.3 nm
500.0 nm

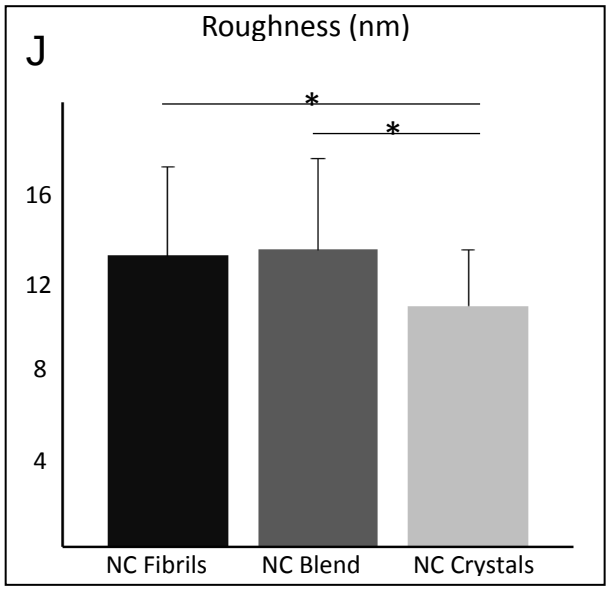
J
Roughness (nm)
*
*
16
12
8
4
NC Fibrils
NC Blend
NC Crystals

Fig. 2. AFM analysis of **(A-C)** NC fibrils, **(D-F)** CNCs and **(G-I)** NC blend. **(J)** Surface roughness of NC fibrils, blend and crystals. The level of statistical significance was set at * $p < 0.05$.

3.1.2. Porosity.

Cryo-SEM was used to analyse the surface morphology, and nano- and microstructure of NC fibrils, crystals and a blend (Fig. 3). Micrographs obtained from NC fibrils showed extensive porous fibrillar networks with varying void sizes (Fig. 3A-B). These pore sizes (measured using image analysis software) ranged from 104 nm to over 45 μm in diameter with a mean diameter of 2827 nm (**Table 2**). Micrographs obtained from CNCs revealed a densely-packed network of randomly oriented rod-like structures with reduced porosity (Fig. 3C-D). Pore sizes were much smaller, which was clearly evident from the micrographs and measurements. This is thought to be due to the smaller mean diameters of the CNCs compared to the fibrils. It is known that the mean pore size of fibrous networks is related to the width of the fibers (Eichhorn & Sampson, 2005). Pore sizes therefore ranged from 87 to 1609 nm in diameter with a mean diameter of 299 nm. Micrographs of the NC blend highlighted a combination of nano/microstructures with areas of porosity attributed to the loosely-packed NC fibrils surrounding more packed, less porous regions of CNCs (Fig. 3E-F). Quantitatively, the blend had pore diameters ranging from 55 nm to over 12 μm with a mean diameter of 934 nm. In analysing pore size distributions, it was evident that NC fibrils showed a multimodal distribution of pore diameters with the largest variation (**Fig. 4**). Approximately 40% of pore diameters were in the range 100 – 750 nm, ~50% were in the range 750 – 5000nm and ~10% had diameters greater than 5000 nm. Networks of CNCs had pore diameters that were normally distributed with approximately 85% in the range 100 – 500 nm, which correlates with the micrographs. More variation in pore size was evident in the NC blend than crystals. Wider variation was seen with the NC fibrils and the blend. The largest distribution of pore sizes (~70%) were in the range 100 – 750 nm and ~4% had diameters greater than 5000 nm (Fig. 4).

Controlling porosity of NC networks is essential for many applications, especially tissue engineering where it can influence cell adhesion, migration, proliferation and differentiation; with different pore sizes influencing different cellular processes (Harley et al., 2008; Smith, Liu, Smith, & Ma, 2009). A wide variation in the pore sizes may both encourage cell adhesion and migration within the porous networks, a desirable property for a tissue engineering material. The NC crystal nano-surface (~100 nm) is a characteristic shown to be important for the formation of collagen fibers and ECM, whereas the micro- and macro surfaces (100 nm – 100 μm) of the NC fibril formulation plays an important role in cell seeding, distribution, migration and *in vivo* neo-vascularisation, but lacks the nanopores for optimal cell attachment and function (Bružauskaitė, Bironaitė, Bagdonas, & Bernotienė, 2016; Smith et al., 2009). The broader variation in pore sizes of the NC blend formulation (Fig. 4) may provide a greater variety of bioactive signals for tissue engineering. Through modifying the surface topography by blending different formulations of NC fibrils and CNCs, it may be possible to control adhesion and differentiation of a variety of cell types. For example, osteoblasts have been shown to attach and proliferate better on rougher surfaces (200 nm) but show increased osteogenic differentiation in response to larger pore sizes (5 – 8 μm) (Hatano et al., 1999; Lee et al., 2004).

For many applications, controlled permeability and high surface area are important properties. One study found that through careful control of processing conditions, porosity can range from 40 – 86% with remarkably small pore diameters in the range 5 – 100 nm which show potential for membrane applications (Sehaqui, Zhou, Ikkala, & Berglund, 2011). In another study which showed potential for NC implants in cartilage tissue engineering, bovine chondrocytes were seeded into bacterial NC hydrogels and ingrowth was found to be limited due to small pore size and heterogeneity (Ahrem et al., 2014).

Table 1

Dimensions of NC fibrils, CNCs and blend determined from TEM measurements.

	NC fibrils		CNCs		NC blend	
	Width (nm)	Length (nm)	Width (nm)	Length (nm)	Width (nm)	Length (nm)
Mean (nm)	29 ± 18	1627 ± 1252	4.5 ± 1.5	222 ± 139	17 ± 12	925 ± 787
Mode (nm)	12	420	5.7	168	12	275
Median (nm)	24	1009	4.4	185	8.2	420
Aspect ratio	55		49		55	

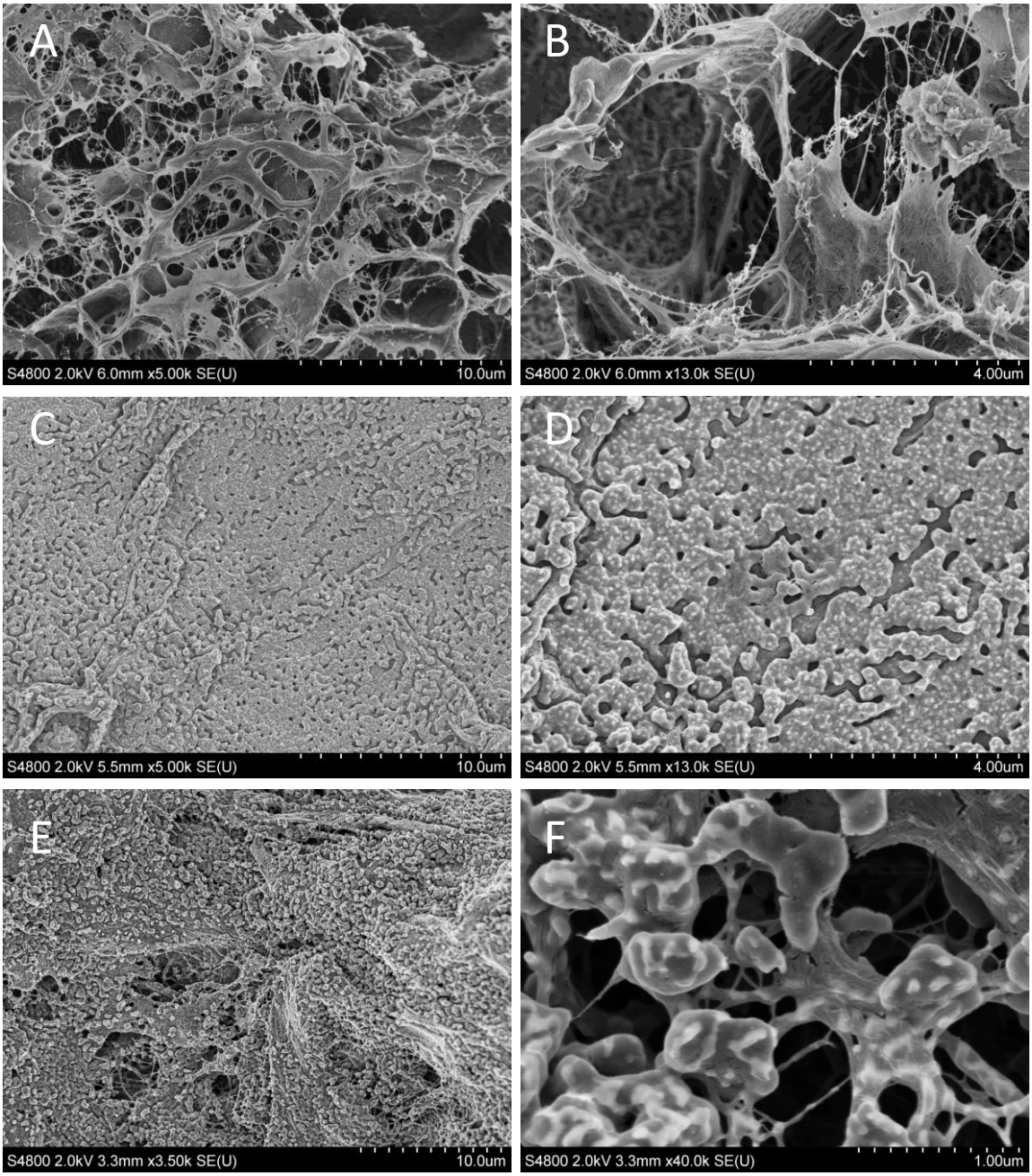

Fig. 3. Cryo-SEM analysis of **(A-B)** NC fibrils, (**C-D)** CNCs and **(E-F)** NC blend.

Table 2

Pore size analysis of NC fibrils, CNCs and blend.

	Pore diameter (nm)			
	Mean	Maximum	Minimum	Median
NC fibrils	2827	45876	104	1045
CNCs	299	1609	87	211
NC blend	934	12141	55	454

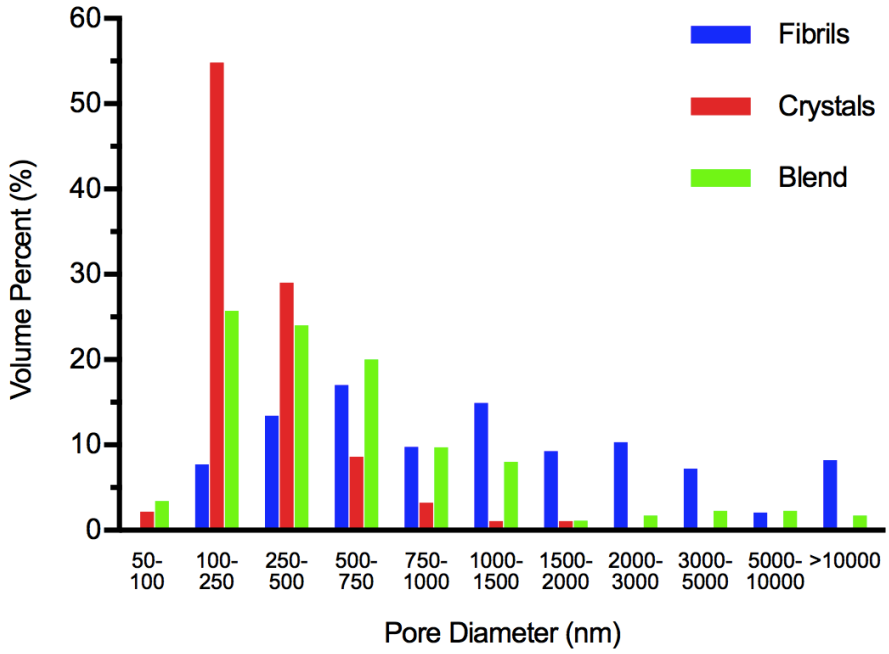

Fig. 4. Pore size distribution of NC fibrils, crystals (CNCs) and blend.

3.2. FTIR analysis.

It is evident from the FTIR spectra in **Fig. 5** that little difference is seen between the individual bond vibrations within NC fibrils, CNCs and the blend, other than changes in intensity. The broad band located at ~3400 cm^{-1} (Label 1) was observed in all samples and was attributed to hydrogen bonding of the O-H stretching vibration which indicates the hydrophilic tendency of NC (Cintil Jose Chirayil et al., 2014). The band located at ~2883 cm^{-1} is assigned to the aliphatic C-H stretching vibration (Label

2). Low intensity bands located at ~1623 cm^{-1} (Label 3), ~1425 cm^{-1} (Label 4), ~1370 cm^{-1} (Label 5), ~1160 cm^{-1} (Label 6) and ~1088 cm^{-1} (Label 7) are assigned to the bending vibration of the OH bond in absorbed water, CH_2 symmetric bending, CH bending, C-O-C stretching and out-of-phase bending, respectively. The intense band noted at ~1025 cm^{-1} is associated with C-C, C-OH and C-H ring and side group vibrations (Label 8). A small band located at ~892 cm^{-1} is attributed to C-O-C, C-C-O and C-C-H deformation and stretching vibrations (Label 9). This band represents the glycosidic $^4C_1$ ring conformation deformation and the β-glycosidic linkages between glucopyranose rings in cellulose (Cintil Jose Chirayil et al., 2014). The band located at ~1425 cm^{-1} (Label 4) is associated with the amount of crystalline structure within cellulose, while the band at ~892 cm^{-1} (Label 8) is assigned to the amorphous regions of cellulose (Åkerholm, Hinterstoisser, & Salmén, 2004). A summary of absorbance/transmission signals associated with bond vibrations within NC is highlighted in **Table 3**. The results observed in this study were consistent with other FTIR data for NC found in the literature (Y. W. Chen, Lee, Juan, & Phang, 2016).

FTIR was also used to show that lignin had been removed during the chemical pre-treatment steps. There are several bands attributed to functional groups indicative of the presence of lignin that are not evident in the FTIR spectra of NC fibrils, CNCs or the blend in Fig. 5. These include the intramolecular hydrogen bond in a phenolic group in lignin at ~3570 cm^{-1} (C.-M. Popescu et al., 2009), C=O stretching in conjugated *p*-substituted aryl ketones in the range 1715 – 1675 cm^{-1}, C=C stretching of the aromatic guaiacyl and syringyl rings in the range 1602 – 1502 cm^{-1}, guaiacyl ring breathing and C-O linkage in guaiacyl aromatic methoxyl groups at ~1268 cm^{-1}, and C-H out of plane vibrations in positions 2, 5 and 6 of guaiacyl units in the range 843 – 835 cm^{-1} (Kubo & Kadla, 2005; C. Popescu et al., 2006; Wang et al., 2009). It should also be noted that the presence of lignin would not diminish the potential for NC-based material applications. AVAP® technology can also produce lignin-coated NC materials for a range of applications, and it has been well documented that incorporation of lignin into nanocellulose can improve hydrophobicity which can make such materials more compatible with non-polar polymers such as polyethylene and polypropylene (Rosa et al., 2010), and enhance impact resistance (Agrawal, Kaushik, & Biswas, 2014).

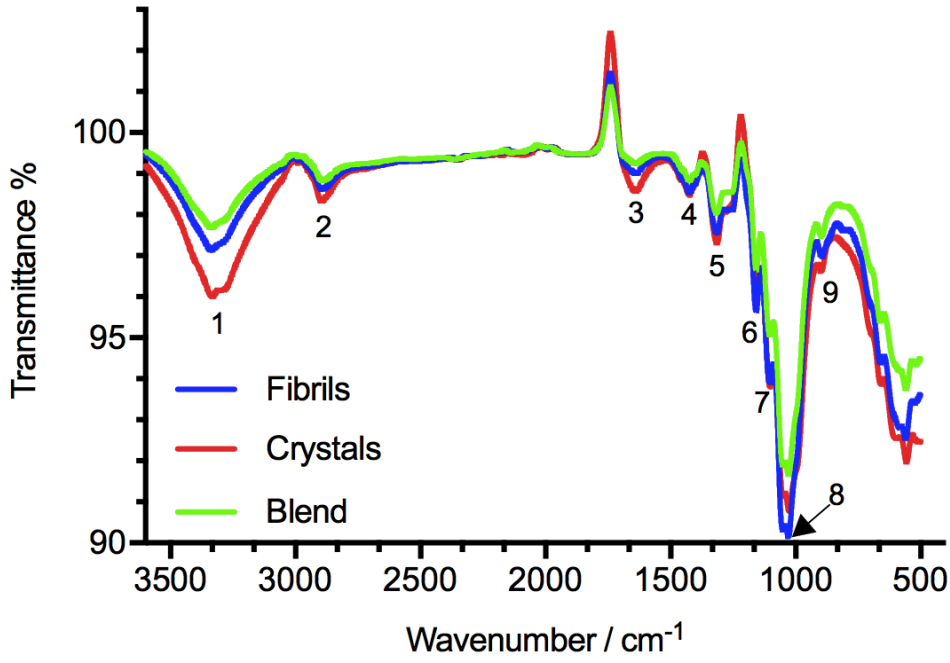

Fig. 5. FTIR spectrum of NC fibrils, crystals (CNCs) and blend.

Table 3

Infra-red band assignments for NC structures.

Wavenumber range / cm^{-1}	Bonds
3500 – 3200	OH stretching
3000 – 2835	C-H stretching
1652 – 1623	OH bending of absorbed water
1470 – 1420	C-H bending
1391 – 1368	C-H and C-O vibrations in pyranose ring
1260 – 1150	C-O-C stretching
1111 – 1056	Out-of-phase bending
1046 – 994	C-C, C-OH, C-H ring and side group vibrations
898 – 890	COC, CCO and CCH deformation and stretching

3.3. X-ray diffraction analysis.

X-ray diffraction was used to characterize the crystal structures of NC fibrils, CNCs and blend. The diffractograms are shown in **Fig. 6**. Two main diffraction peaks can be seen in all NC samples. The first occurs at 2θ = 15.5 ° and the second at 2θ = 22.5 ° which correspond to the overlap of peaks assigned to crystallographic planes (110) and ($1\bar{1}0$), and (200) respectively. These polymorphs correspond to the cellulose I structure which is characterized with a parallel arrangement of two anhydroglucose chains and has been referred to as the polymorph of cellulose with the highest mechanical integrity (Paakko et al., 2007). A low intensity peak can also be observed at 2θ = 34 °, which corresponds to the plane (004) of cellulose.

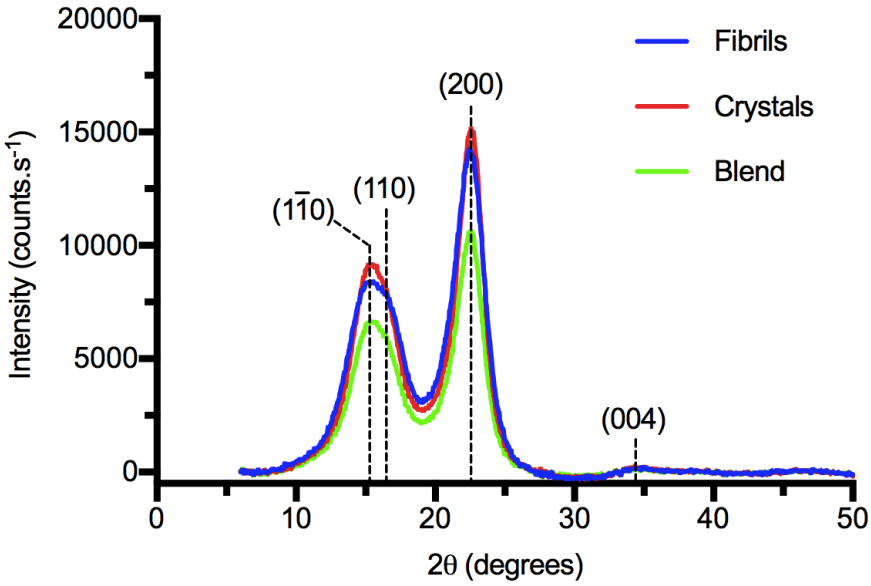

Fig. 6. X-ray diffraction pattern of NC fibrils, crystals (CNCs) and blend.

3.4. Thermal stability.

The thermogravimetric analysis (in a nitrogen environment) of NC fibrils, CNCs and the blend is shown in **Fig. 7**. The onset of decomposition and peak decomposition (maximum rate) temperatures are highlighted in **Table 4**. The decomposition onset and maximum rate of decomposition temperatures was observed in the sequence CNCs > NC blend > NC fibrils. Hence the CNCs showed an enhanced thermal stability compared to the NC blend and fibrils. The thermal stability profiles of NC highlighted in this study were comparable to, and often more thermally stable than those

previously reported (Cho & Park, 2011; Rusmirović et al., 2017). One study found that incorporation of greater than 5 wt% microcrystalline cellulose into poly (vinyl alcohol) nanocomposites increased thermal stability, whilst concentrations below this had no significant influence (Cho & Park, 2011). In another study, incorporation of 5 wt% CNCs into thermoplastic starches enhanced thermal stability which may prove useful for short-life applications in the food packaging industry (Montero, Rico, Rodríguez-Llamazares, Barral, & Bouza, 2017).

The advantage of using AVAP® technology to produce such NC materials is that the process is free from sulfuric acid hydrolysis and hence NC fibrils are not functionalized with sulfate half ester groups, as they have been with more traditional methods of CNC production. It is well documented in the literature that such functionalization lowers thermal stability (Roman & Winter, 2004; Rosa et al., 2010; Zhou et al., 2012). The replacement of hydroxyl groups by sulfated groups during acid hydrolysis reduces the activation energy for degradation due to dehydration, making them less resistant to pyrolysis, and subsequently making CNCs more susceptible to degradation at higher temperatures (Costa et al., 2015). Furthermore, CNCs produced during acid hydrolysis have a greater number of free chain ends due to their smaller particle size, and decomposition of these chain ends starts at lower temperatures (Staggs, 2006). For tissue engineering applications, it is therefore evident that NC can be used at physiological temperature (37 ºC) and all three formulations (fibril, CNCs and blend) remain stable well above the 121 ºC autoclave temperatures used for sterilization. However, a small amount of moisture loss was noted between 50 – 140 ºC in all NC samples and it would be important to investigate the effect of autoclaving or other potential sterilization techniques on fiber nano- and microarchitecture, as well as porosity.

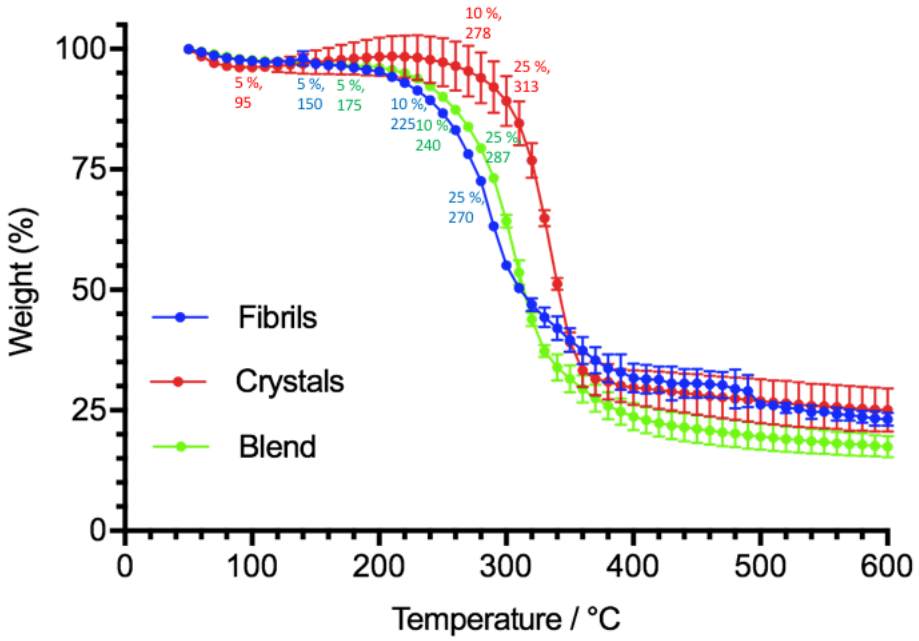

Fig. 7. Thermogravimetric analysis of NC fibrils, crystals (CNCs) and blend showing the weight losses at 5, 10 and 25 wt % with the corresponding temperatures.

Table 4

Thermal decomposition temperatures of NC fibrils, crystals (CNCs) and blend.

	NC Fibrils	CNCs	NC blend
Onset of decomposition temperature (T_{on})/°C	246.8 ± 3.0	298.8 ± 4.9	265. 4 ± 2.9
Maximum rate of decomposition temperature (T_{max})/°C	291. 7 ± 1.5	337.3 ± 3.8	309.3 ± 7.4

3.5. Surface charge analysis.

Surface charge was evaluated by means of the zeta potential which measures the mobility of charged particles across an electric field. All NC samples in neutral

water showed a negative zeta potential. The average zeta potential was determined to be -23.3 ± 5.4 mV, which highlights that the NC suspensions are stable colloids. Understanding and manipulating surface charge is critical for most applications involving material-aqueous interfaces, such as protein adsorption, biofilm formation, drug delivery and biodistribution. In the biomaterials context, surface charge at the solid/water interface determines the electrostatic interaction between the biomaterial surface and the soluble ions, molecules and proteins from the biological environment, leading to the formation of an adsorbed protein layer that influences cell adhesion (Espanol, Mestres, Luxbacher, Dory, & Ginebra, 2016). Negatively charged biomaterials are less likely to be internalized by cells than those that are neutral or positively charged when other parameters such as shape and size of the nanoparticles are comparable (L. Chen, McCrate, Lee, & Li, 2011).

The AVAP® process does not introduce functional groups onto the surface, unlike other methods that use sulfuric acid hydrolysis thereby resulting in higher zeta potentials due to the anionic sulfate half ester groups added to the surface (Kim & Song, 2015). Often the size of the zeta potentials are proportional to the length of acid hydrolysis owing to the increase in sulfate ions (Eyley & Thielemans, 2011; Kargarzadeh et al., 2012). The NC fibrils, CNCs and blend obtained in this study comprise pure cellulose with negligible sulfur content (NC fibrils: 0.022%, CNCs: 0.023%, blend: 0.023%). In biomedicine, sulfur-containing nanoparticles have been found to be cytotoxic to mammalian cells in a concentration dependent manner (Jeong, Oh, Kim, & Jang, 2011). A greater understanding of the *in vitro* and *in vivo* toxicological profiles of NC-based materials, especially those with surface modifications will be essential for the potential cell-based therapies this promising cellulosic material could offer.

The lack of post-hydrolysis modifications on the NC preparations in this study allows facile surface functionalization of the three hydroxyl groups resulting in promising potential for novel, advanced and multifunctional nanomaterials with improved biocompatibility and tissue generation (Bodin et al., 2007). The concept of cellulose surface modification is not new since oxidation of cellulose creating 6-carboxycellulose has been used for over seventy years in applications that range from wound dressing gauzes to hemostatic agents. Advances in organic chemistry, in particular click chemistry, has allowed various cellulose nanostructures to be modified and decorated with a plethora of molecules for a range of applications. The polyol

nature of NC materials allows for limitless chemical functionalization that can potentially change hydrophilicity, aggregation state and hierarchical organization (Habibi et al., 2010). Therefore, better manipulation of NC surface charge and chemistry may pave the way in developing smart, adaptable functionalized nanomaterials.

3.6. Rheology.

The storage (elastic) modulus, (G'), loss (viscous) modulus (G''), shear viscosity as a function of shear rate, and the tangent of the phase angle (loss tangent) $\tan\delta = \frac{G''}{G'}$ are shown in **Fig. 8**. The storage modulus is greater than the loss modulus for all NC samples over all frequencies studied indicating a dominance of elasticity in these systems and demonstrating the presence of relatively strong interconnecting networks between nanostructures (Fig. 8A, B). The rigidity of the NC hydrogels follows the sequence: NC blend > NC fibrils > CNCs. This is an interesting finding insofar that the NC blend produced a material with increased rigidity than NC fibrils or CNCs alone, suggesting that each component of the nanostructures combines to reinforce the resulting network (Nakajima et al., 2009). This is further supported by imaging studies reported earlier.

Shear rate ramps were performed to investigate the flow properties of NC fibrils, CNCs and NC blend by measuring the viscosity as a function of increasing shear rate (Fig. 8C). All NC samples showed strong non-Newtonian, shear thinning (pseudoplastic) behaviour with the viscosity being highest in the NC blend over the entire shear rates studied. This implies that there are stronger particle-particle interactions or increased entanglements between nano- and microstructures within the NC blend compared to the NC fibrils and CNCs which would provide a better shape fidelity during bioprinting (Markstedt et al., 2015). The origin of the shear thinning can be associated with the orientation of the NC nanostructures in the direction of shear flow as shown in Fig. 8C. Nanostructures are coiled at lower shear rates, and as this rate increases, the nanostructures disentangle until they are fully separate and their axis is aligned parallel to the direction of flow, inducing the existence of an upper Newtonian plateau in the flow curve (Bettaieb et al., 2015; Chirayil, Mathew, Hassan, Mozetic, & Thomas, 2014; Orts, Godbout, Marchessault, & Revol, 1998). In other

words, there may be further shear thinning at higher shear rates with alignment and ordering of individual nanostructures (Orts et al., 1998). This behaviour and concept has also been reported by others (C. J. Chirayil et al., 2014; Li et al., 2015; Ureña-Benavides, Ao, Davis, & Kitchens, 2011). The shear thinning properties of nanocellulose gels are particularly useful in 3D bioprinting applications (Markstedt et al., 2015).

Predominantly viscous fluids show tan $\delta > 1$, i.e. the loss modulus is greater than the storage modulus, whereas more elastic materials show tan $\delta < 1$, i.e. where the storage modulus is greater than the loss modulus. All NC samples showed dominant elastic behaviour over the entire frequency range studied (Fig. 8D), which is typical of highly entangled systems (Kavanagh & Ross-Murphy, 1998). Interestingly, tan δ is relatively constant between each NC sample which implies that underlying structural integrity appears to be preserved.

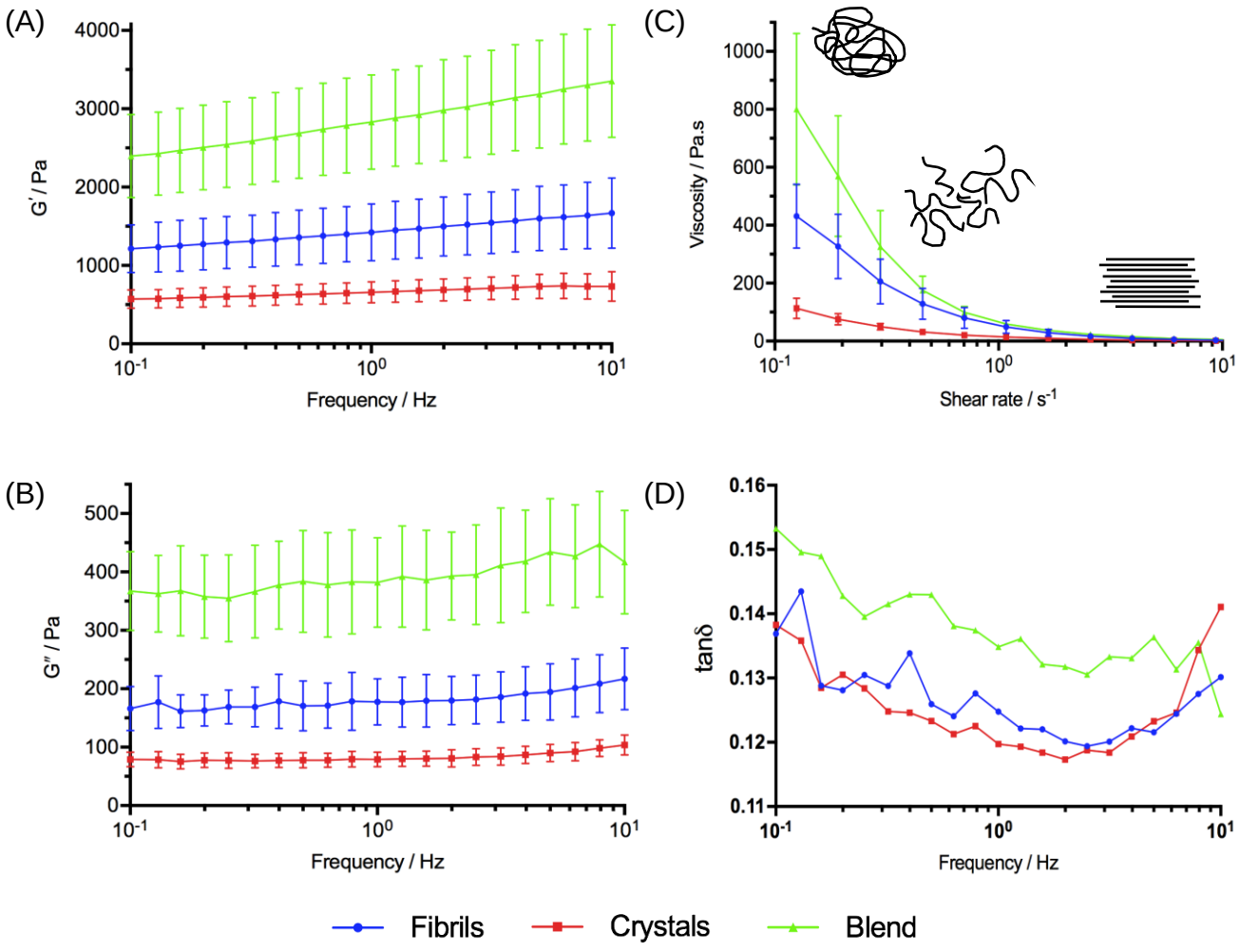

Fig. 8. Viscoelastic measurements of NC fibrils, crystals (CNCs) and blend. (A) Storage modulus (G'), (B) loss modulus (G''), (C) viscosity as a function of shear rate and (D) loss tangent (tan $\delta=\frac{G''}{G'}$).

4. Conclusions

Previous characterization studies have shown NC materials to have favourable properties for diverse applications. Many studies investigating the use of NC for a variety of applications have been very promising but focused on bacterial rather than pulp-derived forms which are limited by high processing costs and low product yield.

In this study, we were able to show that all three pulp-derived NC formulations (fibril, crystal, and blends) were pure cellulose I structures, free of lignin. For applications requiring high temperatures, thermal stability was well above the 121 °C temperature normally used for steam autoclaving. Surface charge analysis revealed stable colloid suspensions with a negative surface charge (-23.3 ± 5.4 mV). The lack of post-hydrolysis modifications provides exciting implications for functionalization with various molecules, as well as the ability to combine with various natural and synthetic matrices to develop enhanced (bio)composites.

Morphologically, NC exhibited a nano- and microarchitecture with variable porosity and uniformly high aspect ratio. The fibrils formed complex entanglements with lengths measured in the micron range and nano widths. The CNC network exhibited a compact packing of nanorods with reduced porosity. The unique NC blend exhibited a combination of porous fibrillar networks and interconnecting compact nanorods similar to that described in the literature for bacterial NC. Exhibiting both nano- and micro-roughness may be useful in surface coatings and in tissue engineering where cellular adhesion, proliferation, differentiation and tissue formation are important. Rheological studies highlighted a dominance of elasticity in all variants, with the NC blend being more rigid than the NC fibrils and CNCs, indicating a double network hydrogel structure. The higher strength may be due to the interconnection between the two networks through covalent bonds and may be further strengthened through crosslinking. This could be useful for biomimetic tissue engineering scaffolds where the mechanical properties of native tissue can be closely matched. In bioprinting

applications, the higher overall viscosity of NC blend versus fibrils or crystals indicates potential to better replicate micro- and macro-architecture of native tissue due to improved shape fidelity. The NC hydrogels were also shear thinning which is particularly useful in a range of coating applications.

Undoubtedly, nanocellulose has great potential for the breakthrough of a novel generation of (bio)nanomaterials. To realise the full potential of nanocellulose, it is important to control properties with reliable and reproducible production techniques. Nanocellulose preparations made using AVAP® technology offers the potential for cost-effective, commercial-scale production of NC alongside flexibility in final product morphology, surface properties and elasticity through NC blend formulations. This adaptable process has the potential to influence a wide range of (bio)nanotechnological applications which will be enhanced through strong collaborations between academia, industry, government institutions, engineers, material scientists and clinicians.

Acknowledgements

The authors would like to acknowledge the following institutions for their support of this work: Royal College of Surgeons of England: Pump Priming Award for Consultants (to I.S.W), Research Fellowship (to Z.M.J), Clarke Medal (to I.S.W/Z.M.J/A.A), British Association of Plastic, Reconstructive and Aesthetic Surgeons: Pump Priming Award (to I.S.W/Z.M.J), Medical Research Council: Clinical Research Training Fellowship (to Z.M.J), Welsh Assembly Government: Welsh Clinical Academic Training Pathway (to Z.M.J), ABMU Health Board: Capacity Building Award (to I.S.W), Oak Grove Medical Foundation: Research Award (to I.S.W) and St David's Foundation: Research Start-up (to A.A)

References

Abdul Khalil, H. P. S., Bhat, A. H., & Ireana Yusra, A. F. (2012). Green composites from sustainable cellulose nanofibrils: A review. *Carbohydrate Polymers,* 87(2), 963-979.

Abitbol, T., Rivkin, A., Cao, Y., Nevo, Y., Abraham, E., Ben-Shalom, T., . . . Shoseyov, O. (2016). Nanocellulose, a tiny fiber with huge applications. *Curr Opin Biotechnol,* 39, 76-88.

Agrawal, A., Kaushik, N., & Biswas, S. (2014). Derivatives and Applications of Lignin–An Insight. *The SciTech Journal,* 1, 30-36.

Ahrem, H., Pretzel, D., Endres, M., Conrad, D., Courseau, J., Muller, H., . . . Kinne, R. W. (2014). Laser-structured bacterial nanocellulose hydrogels support ingrowth and differentiation of chondrocytes and show potential as cartilage implants. *Acta Biomater,* 10(3), 1341-1353.

Amiralian, N., Annamalai, P. K., Memmott, P., Taran, E., Schmidt, S., & Martin, D. J. (2015). Easily deconstructed, high aspect ratio cellulose nanofibres from Triodia pungens; an abundant grass of Australia's arid zone. *RSC Advances,* 5(41), 32124-32132.

Bettaieb, F., Nechyporchuk, O., Khiari, R., Mhenni, M. F., Dufresne, A., & Belgacem, M. N. (2015). Effect of the oxidation treatment on the production of cellulose nanofiber suspensions from Posidonia oceanica: The rheological aspect. *Carbohydr Polym,* 134, 664-672.

Bodin, A., Ahrenstedt, L., Fink, H., Brumer, H., Risberg, B., & Gatenholm, P. (2007). Modification of nanocellulose with a xyloglucan-RGD conjugate enhances adhesion and proliferation of endothelial cells: implications for tissue engineering. *Biomacromolecules,* 8(12), 3697-3704.

Bružauskaitė, I., Bironaitė, D., Bagdonas, E., & Bernotienė, E. (2016). Scaffolds and cells for tissue regeneration: different scaffold pore sizes—different cell effects. *Cytotechnology,* 68(3), 355-369.

Capadona, J. R., Shanmuganathan, K., Tyler, D. J., Rowan, S. J., & Weder, C. (2008). Stimuli-responsive polymer nanocomposites inspired by the sea cucumber dermis. *Science,* 319(5868), 1370-1374.

Capadona, J. R., Van Den Berg, O., Capadona, L. A., Schroeter, M., Rowan, S. J., Tyler, D. J., & Weder, C. (2007). A versatile approach for the processing of polymer nanocomposites with self-assembled nanofibre templates. *Nat Nanotechnol,* 2(12), 765-769.

Chen, L., McCrate, J. M., Lee, J. C., & Li, H. (2011). The role of surface charge on the uptake and biocompatibility of hydroxyapatite nanoparticles with osteoblast cells. *Nanotechnology,* 22(10), 105708.

Chen, W., Li, Q., Cao, J., Liu, Y., Li, J., Zhang, J., . . . Yu, H. (2015). Revealing the structures of cellulose nanofiber bundles obtained by mechanical nanofibrillation via TEM observation. *Carbohydr Polym,* 117, 950-956.

Chen, Y. W., Lee, H. V., Juan, J. C., & Phang, S.-M. (2016). Production of new cellulose nanomaterial from red algae marine biomass Gelidium elegans. *Carbohydrate Polymers,* 151, 1210-1219.

Cheng, Q., Wang, S., Rials, T. G., & Lee, S.-H. (2007). Physical and mechanical properties of polyvinyl alcohol and polypropylene composite materials reinforced with fibril aggregates isolated from regenerated cellulose fibers. *Cellulose,* 14(6), 593-602.

Chirayil, C. J., Joy, J., Mathew, L., Mozetic, M., Koetz, J., & Thomas, S. (2014). Isolation and characterization of cellulose nanofibrils from Helicteres isora plant. *Industrial Crops and Products,* 59, 27-34.

Chirayil, C. J., Mathew, L., Hassan, P. A., Mozetic, M., & Thomas, S. (2014). Rheological behaviour of nanocellulose reinforced unsaturated polyester nanocomposites. *Int J Biol Macromol,* 69, 274-281.

Cho, M.-J., & Park, B.-D. (2011). Tensile and thermal properties of nanocellulose-reinforced poly(vinyl alcohol) nanocomposites. *Journal of Industrial and Engineering Chemistry,* 17(1), 36-40.

Costa, L. A. S., Assis, D. d. J., Gomes, G. V. P., Silva, J. B. A. d., Fonsêca, A. F., & Druzian, J. I. (2015). Extraction and Characterization of Nanocellulose from Corn Stover. *Materials Today: Proceedings,* 2(1), 287-294.

Dugan, J. M., Gough, J. E., & Eichhorn, S. J. (2013). Bacterial cellulose scaffolds and cellulose nanowhiskers for tissue engineering. *Nanomedicine (Lond),* 8(2), 287-298.

Eichhorn, S. J., & Sampson, W. W. (2005). Statistical geometry of pores and statistics of porous nanofibrous assemblies. *J R Soc Interface,* 2(4), 309-318.

Endes, C., Camarero-Espinosa, S., Mueller, S., Foster, E. J., Petri-Fink, A., Rothen-Rutishauser, B., . . . Clift, M. J. (2016). A critical review of the current knowledge regarding the biological impact of nanocellulose. *J Nanobiotechnology,* 14(1), 78.

Espanol, M., Mestres, G., Luxbacher, T., Dory, J.-B., & Ginebra, M.-P. (2016). Impact of Porosity and Electrolyte Composition on the Surface Charge of Hydroxyapatite Biomaterials. *ACS Applied Materials & Interfaces,* 8(1), 908-917.

Eyley, S., & Thielemans, W. (2011). Imidazolium grafted cellulose nanocrystals for ion exchange applications. *Chemical Communications,* 47(14), 4177-4179.

Freitas Jr, R. A. (1999). *Nanomedicine, Volume 1: Basic Capabilities*. Georgetown, Texas: Landes Bioscience.

Gao, H., Shi, W., & Freund, L. B. (2005). Mechanics of receptor-mediated endocytosis. *Proc Natl Acad Sci U S A,* 102(27), 9469-9474.

Habibi, Y., Lucia, L. A., & Rojas, O. J. (2010). Cellulose nanocrystals: chemistry, self-assembly, and applications. *Chem Rev,* 110(6), 3479-3500.

Harley, B. A., Kim, H. D., Zaman, M. H., Yannas, I. V., Lauffenburger, D. A., & Gibson, L. J. (2008). Microarchitecture of three-dimensional scaffolds influences cell migration behavior via junction interactions. *Biophys J,* 95(8), 4013-4024.

Hatano, K., Inoue, H., Kojo, T., Matsunaga, T., Tsujisawa, T., Uchiyama, C., & Uchida, Y. (1999). *Effect of surface roughness on proliferation and alkaline phosphatase expression of rat calvarial cells cultured on polystyrene*. In *Bone* (pp. 439-445). United States

Hausmann, A., Samans, B., Lill, R., & Muhlenhoff, U. (2008). *Cellular and mitochondrial remodeling upon defects in iron-sulfur protein biogenesis*. In *J Biol Chem* (pp. 8318-8330). United States

Iakovlev, M., You, X., van Heiningen, A., & Sixta, H. (2014). SO2-ethanol-water (SEW) fractionation of spruce: kinetics and conditions for paper and viscose-grade dissolving pulps. *RSC Advances,* 4(4), 1938-1950.

Jeong, Y. S., Oh, W. K., Kim, S., & Jang, J. (2011). Cellular uptake, cytotoxicity, and ROS generation with silica/conducting polymer core/shell nanospheres. *Biomaterials,* 32(29), 7217-7225.

Kamal, M. R., & Khoshkava, V. (2015). Effect of cellulose nanocrystals (CNC) on rheological and mechanical properties and crystallization behavior of PLA/CNC nanocomposites. *Carbohydrate Polymers,* 123, 105-114.

Kargarzadeh, H., Ahmad, I., Abdullah, I., Dufresne, A., Zainudin, S. Y., & Sheltami, R. M. (2012). Effects of hydrolysis conditions on the morphology, crystallinity, and thermal stability of cellulose nanocrystals extracted from kenaf bast fibers. *Cellulose,* 19(3), 855-866.

Kavanagh, G. M., & Ross-Murphy, S. B. (1998). Rheological characterisation of polymer gels. *Progress in Polymer Science,* 23(3), 533-562.

Kim, D. H., & Song, Y. S. (2015). Rheological behavior of cellulose nanowhisker suspension under magnetic field. *Carbohydr Polym,* 126, 240-247.

Kubo, S., & Kadla, J. F. (2005). Hydrogen Bonding in Lignin: A Fourier Transform Infrared Model Compound Study. *Biomacromolecules,* 6(5), 2815-2821.

Kvien, I., Tanem, B. S., & Oksman, K. (2005). Characterization of Cellulose Whiskers and Their Nanocomposites by Atomic Force and Electron Microscopy. *Biomacromolecules,* 6(6), 3160-3165.

Kyle, S., Jessop, Z. M., Al-Sabah, A., & Whitaker, I. S. (2017). 'Printability' of Candidate Biomaterials for Extrusion Based 3D Printing: State-of-the-Art. *Adv Healthc Mater,* 6(16).

Lee, S. J., Choi, J. S., Park, K. S., Khang, G., Lee, Y. M., & Lee, H. B. (2004). *Response of MG63 osteoblast-like cells onto polycarbonate membrane surfaces with different micropore sizes*. In *Biomaterials* (pp. 4699-4707). Netherlands

Li, B., Xu, W., Kronlund, D., Maattanen, A., Liu, J., Smatt, J. H., . . . Xu, C. (2015). Cellulose nanocrystals prepared via formic acid hydrolysis followed by TEMPO-mediated oxidation. *Carbohydr Polym,* 133, 605-612.

Lin, N., Bruzzese, C., & Dufresne, A. (2012). TEMPO-oxidized nanocellulose participating as crosslinking aid for alginate-based sponges. *ACS Appl Mater Interfaces,* 4(9), 4948-4959.

Lu, Z., Fan, L., Zheng, H., Lu, Q., Liao, Y., & Huang, B. (2013). Preparation, characterization and optimization of nanocellulose whiskers by simultaneously ultrasonic wave and microwave assisted. *Bioresource Technology,* 146, 82-88.

Mao, Y., Liu, K., Zhan, C., Geng, L., Chu, B., & Hsiao, B. S. (2017). Characterization of Nanocellulose Using Small-Angle Neutron, X-ray, and Dynamic Light Scattering Techniques. *J Phys Chem B,* 121(6), 1340-1351.

Maret, W. (2004). Zinc and sulfur: a critical biological partnership. *Biochemistry,* 43(12), 3301-3309.

Maret, W., & Krężel, A. (2007). Cellular Zinc and Redox Buffering Capacity of Metallothionein/Thionein in Health and Disease. *Molecular Medicine,* 13(7-8), 371-375.

Markstedt, K., Mantas, A., Tournier, I., Martinez Avila, H., Hagg, D., & Gatenholm, P. (2015). 3D Bioprinting Human Chondrocytes with Nanocellulose-Alginate Bioink for Cartilage Tissue Engineering Applications. *Biomacromolecules,* 16(5), 1489-1496.

Mondal, S. (2017). Preparation, properties and applications of nanocellulosic materials. *Carbohydrate Polymers,* 163, 301-316.

Montero, B., Rico, M., Rodríguez-Llamazares, S., Barral, L., & Bouza, R. (2017). Effect of nanocellulose as a filler on biodegradable thermoplastic starch films from tuber, cereal and legume. *Carbohydrate Polymers,* 157, 1094-1104.

Nakajima, T., Furukawa, H., Tanaka, Y., Kurokawa, T., Osada, Y., & Gong, J. P. (2009). True Chemical Structure of Double Network Hydrogels. *Macromolecules,* 42(6), 2184-2189.

Nascimento, D. M., Almeida, J. S., Dias, A. F., Figueiredo, M. C., Morais, J. P., Feitosa, J. P., & de, F. R. M. (2014). A novel green approach for the preparation of cellulose nanowhiskers from white coir. *Carbohydr Polym,* 110, 456-463.

Nelson, K., & Restsina, T. (2014). Innovative nanocellulose process breaks the cost barrier. *TAPPI Journal,* 13(5), 19-23.

Nelson, K., & Retsina, T. (2014). Innovative nanocellulose process breaks the cost barrier. *TAPPI Journal,* 13(5), 19-23.

Nelson, K., Retsina , T., Iakovlev, M., van Heiningen, A., Deng, Y., Shatkin, J. A., & Mulyadi, A. (2016). *American Process: Production of Low Cost Nanocellulose for Renewable,*

Advanced Materials Applications. In L. D. Madsen & E. B. Svedberg (Eds.), *Materials Research for Manufacturing: An Industrial Perspective of Turning Materials into New Products* (pp. 267-302): Springer International Publishing

Nelson, K., Retsina, T., Pylkkanen, V., & O'Connor, R. (2015). Processes and apparatus for producing nanocellulose, and compositions and products produced therefrom. In USPTO (Ed.), (Vol. US9187865). United States of America: API Intellectual Property Holdings, LLC (Atlanta, GA).

Orts, W. J., Godbout, L., Marchessault, R. H., & Revol, J. F. (1998). Enhanced Ordering of Liquid Crystalline Suspensions of Cellulose Microfibrils: A Small Angle Neutron Scattering Study. *Macromolecules,* 31(17), 5717-5725.

Paakko, M., Ankerfors, M., Kosonen, H., Nykanen, A., Ahola, S., Osterberg, M., . . . Lindstrom, T. (2007). Enzymatic hydrolysis combined with mechanical shearing and high-pressure homogenization for nanoscale cellulose fibrils and strong gels. *Biomacromolecules,* 8(6), 1934-1941.

Peng, B. L., Dhar, N., Liu, H. L., & Tam, K. C. (2011). Chemistry and applications of nanocrystalline cellulose and its derivatives: A nanotechnology perspective. *The Canadian Journal of Chemical Engineering,* 89(5), 1191-1206.

Popescu, C., Vasile, C., Popescu, M., Singurel, G., Popa, V. I., & Munteanu, B. S. (2006). Analytical methods for lignin characterization. II. Spectroscopic studies. *Cellulose chemistry and technology,* 40(8), 597.

Popescu, C.-M., Singurel, G., Popescu, M.-C., Vasile, C., Argyropoulos, D. S., & Willför, S. (2009). Vibrational spectroscopy and X-ray diffraction methods to establish the differences between hardwood and softwood. *Carbohydrate Polymers,* 77(4), 851-857.

Roman, M., & Winter, W. T. (2004). Effect of sulfate groups from sulfuric acid hydrolysis on the thermal degradation behavior of bacterial cellulose. *Biomacromolecules,* 5(5), 1671-1677.

Roohani, M., Habibi, Y., Belgacem, N. M., Ebrahim, G., Karimi, A. N., & Dufresne, A. (2008). Cellulose whiskers reinforced polyvinyl alcohol copolymers nanocomposites. *European Polymer Journal,* 44(8), 2489-2498.

Rosa, M. F., Medeiros, E. S., Malmonge, J. A., Gregorski, K. S., Wood, D. F., Mattoso, L. H. C., . . . Imam, S. H. (2010). Cellulose nanowhiskers from coconut husk fibers: Effect of preparation conditions on their thermal and morphological behavior. *Carbohydrate Polymers,* 81(1), 83-92.

Rusmirović, J. D., Ivanović, J. Z., Pavlović, V. B., Rakić, V. M., Rančić, M. P., Djokić, V., & Marinković, A. D. (2017). Novel modified nanocellulose applicable as reinforcement in high-performance nanocomposites. *Carbohydrate Polymers,* 164, 64-74.

Sehaqui, H., Zhou, Q., Ikkala, O., & Berglund, L. A. (2011). Strong and Tough Cellulose Nanopaper with High Specific Surface Area and Porosity. *Biomacromolecules,* 12(10), 3638-3644.

Shanmuganathan, K., Capadona, J. R., Rowan, S. J., & Weder, C. (2010). Stimuli-responsive mechanically adaptive polymer nanocomposites. *ACS Appl Mater Interfaces,* 2(1), 165-174.

Smith, I. O., Liu, X. H., Smith, L. A., & Ma, P. X. (2009). Nanostructured polymer scaffolds for tissue engineering and regenerative medicine. *Wiley Interdiscip Rev Nanomed Nanobiotechnol,* 1(2), 226-236.

Somerville, C., Bauer, S., Brininstool, G., Facette, M., Hamann, T., Milne, J., . . . Youngs, H. (2004). *Toward a systems approach to understanding plant cell walls*. In *Science* (pp. 2206-2211). United States

Staggs, J. E. J. (2006). Discrete bond-weighted random scission of linear polymers. *Polymer,* 47(3), 897-906.

Sun, X., Wu, Q., Lee, S., Qing, Y., & Wu, Y. (2016). Cellulose Nanofibers as a Modifier for Rheology, Curing and Mechanical Performance of Oil Well Cement. *Sci Rep,* 6, 31654.

Ureña-Benavides, E. E., Ao, G., Davis, V. A., & Kitchens, C. L. (2011). Rheology and Phase Behavior of Lyotropic Cellulose Nanocrystal Suspensions. *Macromolecules,* 44(22), 8990-8998.

Wang, S., Wang, K., Liu, Q., Gu, Y., Luo, Z., Cen, K., & Fransson, T. (2009). Comparison of the pyrolysis behavior of lignins from different tree species. *Biotechnology Advances,* 27(5), 562-567.

Yarbrough, J. M., Zhang, R., Mittal, A., Vander Wall, T., Bomble, Y. J., Decker, S. R., . . . Ciesielski, P. N. (2017). Multifunctional Cellulolytic Enzymes Outperform Processive Fungal Cellulases for Coproduction of Nanocellulose and Biofuels. *ACS Nano,* 11(3), 3101-3109.

Zhou, Y. M., Fu, S. Y., Zheng, L. M., & Zhan, H. Y. (2012). Effect of nanocellulose isolation techniques on the formation of reinforced poly(vinyl alcohol) nanocomposite films. *eXPRESS Polym Lett,* 6(10), 794-804.

Åkerholm, M., Hinterstoisser, B., & Salmén, L. (2004). Characterization of the crystalline structure of cellulose using static and dynamic FT-IR spectroscopy. *Carbohydrate Research,* 339(3), 569-578.